Chinese Chemical Letters 36 (2025) 110311

Contents lists available at ScienceDirect

Chinese Chemical Letters

journal homepage: www.elsevier.com/locate/cclet

Construction of a three-step sequential energy transfer system with selective enhancement of superoxide anion radicals for photocatalysis

Yusong Bi, Rongzhen Zhang, Kaikai Niu, Shengsheng Yu, Hui Liu, Lingbao Xing*

School of Chemistry and Chemical Engineering, Shandong University of Technology, Zibo 255000, China

ARTICLE INFO

Article history:
Received 14 May 2024
Revised 16 July 2024
Accepted 31 July 2024
Available online 2 August 2024

Keywords:
Light-harvesting
Sequential energy transfer
AIE
ROS
Photocatalysis

ABSTRACT

Achieving artificial simulations of multi-step energy transfer processes and conversions in nature remains a challenge. In this study, we present a three-step sequential energy transfer process, which was constructed through host-guest interactions between a piperazine derivative (PPE-BPI) with aggregation-induced emission (AIE) and cucurbit[7]uril (CB[7]) in water to serve as ideal energy donors. To achieve multi-step sequential energy transfer, we employ three distinct fluorescent dyes Eosin B (EsB), Sulforhodamine 101 (SR101), and Cyanine 5 (Cy5) as energy acceptors. The PPE-PBI-2CB[7]+EsB+SR101+Cy5 system demonstrates a highly efficient three-step sequential energy transfer mechanism, starting with PPE-PBI-2CB[7] and transferring energy successively to EsB, SR101, and finally to Cy5, with remarkable energy transfer efficiencies. More interestingly, with the progressive transfer of energy in the multi-step energy transfer system, the generation efficiency of superoxide anion radical ($O_2^{\bullet-}$) increased gradually, which can be used as photocatalysts for selectively photooxidation of *N*-phenyltetrahydroisoquinoline in an aqueous medium with a high yield of 86% after irradiation for 18 h. This study offers a valuable investigation into the simulation of multi-step energy transfer processes and transformations in the natural world, paving the way for further research in the field.

The light-harvesting system (LHS) is an essential element of the natural photosynthesis process and consists of a highly structured arrangement of many antenna molecules [1–4]. The efficient assimilation of photons by the antenna molecules serves as the basis for the chemical conversion of solar energy in the process of photosynthesis. The energy transfer in photosynthesis is achieved through the synchronized cooperation of many antenna molecules. After the antenna molecules absorb photons and gain energy, they transfer the energy to the chromophores in a sequential manner until it finally reaches the reaction center. The energy transmission process can be accomplished by various means, mostly determined by the distance, spatial alignment, and physical properties of the antenna molecules. Fluorescence resonance energy transfer (FRET) is the main energy transfer mechanism that is of particular importance in photosynthesis [1].

In the past few years, scientists have employed the characteristics of supramolecular self-assembly, such as its straightforward construction, efficient assembly, and precise control over structure and function, to develop different supramolecular assemblies for artificial light-harvesting systems (ALHSs) [5–16]. The included assemblies consist of metal coordination assemblies, supramolecular polymers, spherical nanoaggregates, host-guest molecular assemblies, micelles, and vesicles [17–43]. The supramolecular assembly system, created by noncovalent bond interactions and spatial structural effects, may efficiently distribute fluorescent molecules and reduce energy loss due to chromophore aggregation. In addition, it can enhance the efficiency of FRET by ensuring a precise separation between the donor and acceptor molecules inside the supramolecular system. This is accomplished as a result of the system's dynamic and adjustable characteristics, which enable modifications in the internal spatial arrangement and molecule proximity during self-assembly.

Although natural light-harvesting antenna systems are characterized by multi-step sequential energy transfer, the ALHSs mentioned are limited to one or two-step FRET processes. The sequential energy transfer system demonstrates effective long-distance energy transmission without any overlap in spectral characteristics between the donor and acceptor, which exhibits the advantages of versatile tunable fluorescence and effective utilization of light energy [44–46]. Scientists have recently created supramolecular ALHSs by a process of two-step sequential energy transfer. These ALHSs have demonstrated promising potential for use in a wide range of disciplines [47–54]. However, during the process of

* Corresponding author.
E-mail address: lbxing@sdut.edu.cn (L. Xing).

https://doi.org/10.1016/j.cclet.2024.110311
1001-8417/

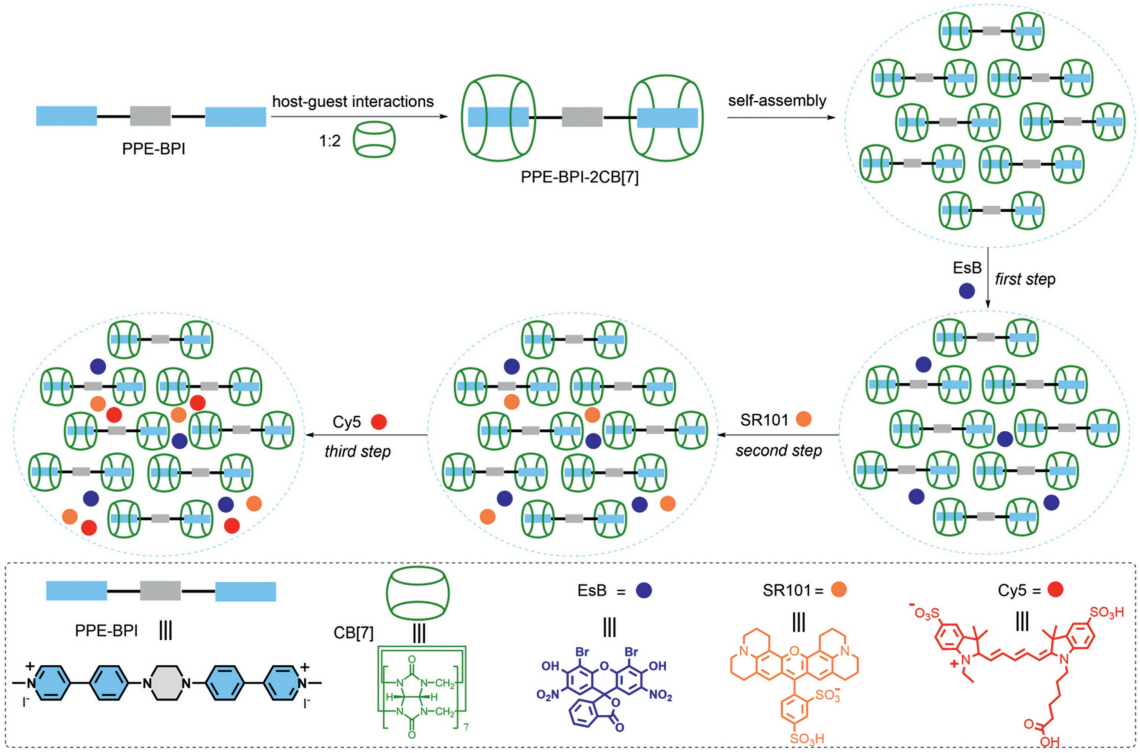

Scheme 1. Schematic illustration of the three-step sequential energy transfer process of PPE-BPI-2CB[7].

photosynthesis, solar energy is captured and transferred *via* many stages until it reaches the reaction center, where it is converted into chemical energy. In order to improve our understanding and ability to recreate photosynthesis, it is crucial to create ALHSs that can efficiently transport energy through various stages and convert light energy into chemical energy. More precisely, an artificial sequential light-harvesting system that employs three or more stages for photocatalysis is of great significance and has been sparsely recorded [55].

In this study, we developed and created a modified piperazine derivative (PPE-BPI) with cationic pyridine units, which has the ability to undergo self-assembly in an aqueous solution, resulting in the formation of PPE-BPI-2CB[7] when interacting with CB[7] through host-guest interactions. PPE-BPI-2CB[7] demonstrated exceptional spectrum characteristics by aggregation-induced emission (AIE). Additionally, it can serve as an energy donor for the creation of ALHSs through sequential energy transfer. To achieve multi-step sequential energy transfer, we employ three distinct fluorescent dyes, specifically Eosin B (EsB), Sulforhodamine 101 (SR101), and Cyanine 5 (Cy5), as energy acceptors (Scheme 1). The PPE-BPI-2CB[7]+EsB+SR101+Cy5 system demonstrates a highly efficient three-step sequential energy transfer process. This process starts with PPE-BPI-2CB[7] and successively transmits energy to EsB, SR101, and finally to Cy5, resulting in exceptional energy transfer efficiencies. Remarkably, as energy is passed along in the multi-step energy transfer system, the effectiveness of producing superoxide anion radical ($O_2^{\bullet-}$) steadily improves. This occurs as the captured energy and reactive oxygen species (ROS) are efficiently utilized in the ALHSs to enhance the photooxidation reaction of *N*-phenyltetrahydroisoquinoline, resulting in a high yield of 86% in water.

PPE-BPI was synthesized using a four-step process (Scheme S1 in Supporting information) and confirmed by ^{1}H NMR and ^{13}C NMR (Figs. S1-S5 in Supporting information). In order to confirm the fluorescence properties of PPE-BPI, the fluorescence emission spectra of PPE-BPI were studied in the mixed solvents of DMSO and water with different ratios, in which its aggregation-induced emission (AIE) behavior can be investigated. As shown in Fig. S6 (Supporting information), PPE-BPI exhibited a very weak emission in DMSO (2.0×10^{-5} mol/L), while the emission increased gradually when the percent of water changed from 0 to 100 vol%. Meanwhile, PPE-BPI emitted sky blue fluorescence when excited at 425 nm in water which could be attributed to the AIE effect of PPE-BPI. The development of the supramolecular complex between PPE-BPI and CB[7] in an aqueous solution was investigated using UV–vis absorption, fluorescence emission spectra, ^{1}H NMR titration, dynamic light scattering (DLS) and zeta potential. As shown in Fig. 1a, the absorption of PPE-BPI at 380 nm dropped gradually and experienced a red shift when CB[7] was added. Meanwhile, the absorption at 425 nm increased gradually with the addition of CB[7]. Moreover, there was a significant rise in the fluorescence intensity of PPE-BPI at 500 nm, which can be attributed to the host-guest interactions between PPE-BPI and CB[7], leading to the creation of a supramolecular complex called PPE-BPI-2CB[7] and accompanying by a change in fluorescence color from sky blue to blue-green (Fig. 1b and Fig. S7 in Supporting information). The fluorescence lifetimes of PPE-BPI-2CB[7] were increased from 0.42 ns (PPE-BPI) to 2.43 ns (Fig. 1c), and the fluorescence quantum yields of PPE-BPI-2CB[7] were increased from 12% (PPE-BPI) to 17% (Table S1 in Supporting information). The binding stoichiometry ratio between PPE-BPI-2CB[7] and CB[7] in the supramolecular complex was determined using Job's plot (Fig. 1d), which revealed that the fluorescence intensity peaked at a molar ratio of 0.33, confirming a stoichiometric ratio of 1:2 between PPE-BPI and CB[7]. Additional ^{1}H NMR experiments were conducted to investigate the interactions between PPE-BPI and CB[7]. These tests showed notable changes in the chemical signals of PPE-BPI protons when 2.0 equiv. of CB[7] was added (Fig. 1e). The self-assembly behavior of PPE-BPI-2CB[7] was further studied by zeta potential and dynamic light scattering (DLS). When CB[7] was added to the PPE-BPI aqueous solution, the

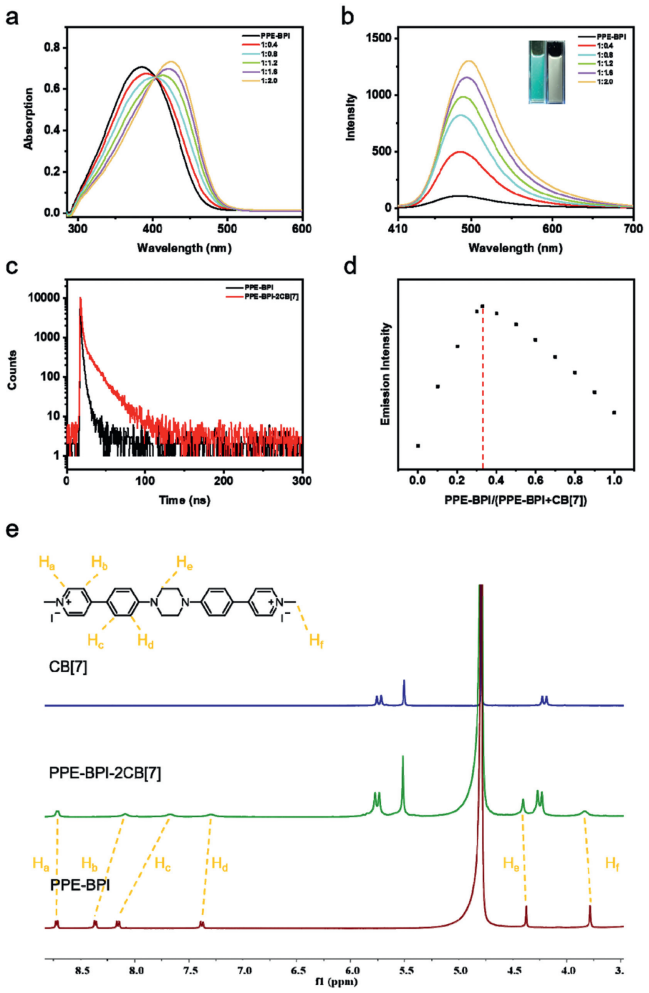

Fig. 1. (a) UV–vis absorption spectra of PPE-BPI with the addition of CB[7]. (b) Fluorescence emission spectra of PPE-BPI with the addition of CB[7], inset: fluorescence colors of PPE-BPI and PPE-BPI-2CB[7]. (c) Fluorescence decay profiles of PPE-BPI and PPE-BPI-2CB[7]. (d) Job's plot for the complexation between PPE-BPI and CB[7]. (e) ^{1}H NMR spectra of PPE-BPI, PPE-BPI-2CB[7], and CB[7].

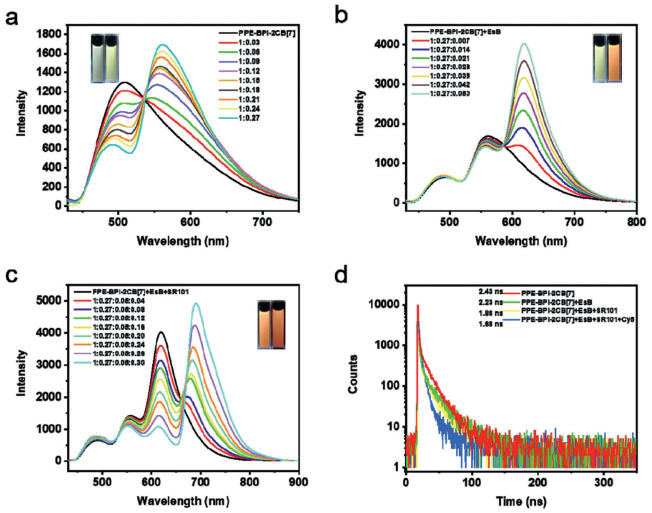

Fig. 2. (a) Fluorescence emission spectra of PPE-BPI-2CB[7] with gradual addition of EsB, inset: fluorescence colors of PPE-BPI-2CB[7] before and after addition of EsB. (b) Fluorescence emission spectra of PPE-BPI-2CB[7]+EsB with gradual addition of SR101, inset: fluorescence colors of PPE-BPI-2CB[7]+EsB before and after addition of SR101. (c) Fluorescence emission spectra of PPE-BPI-2CB[7]+EsB+SR101 with gradual addition of Cy5, inset: fluorescence colors of PPE-BPI-2CB[7]+EsB+SR101 before and after addition of Cy5. (d) Time-resolved fluorescence decay curves of PPE-BPI-2CB[7], PPE-BPI-2CB[7]+EsB, PPE-BPI-2CB[7]+EsB+SR101, and PPE-BPI-2CB[7]+EsB+SR101+Cy5.

zeta potentials increased from −8.49 mV to −2.31 mV, as shown in Fig. S8. At the same time, the size of PPE-BPI-2CB[7] assembly is mainly centered at 350 nm, which indicated the formation of large aggregates. The results all indicate that PPE-BPI and CB[7] form a supramolecular complex through host-guest interactions.

Because of its impressive fluorescence properties in water, PPE-BPI-2CB[7] holds significant promise as an optimal energy donor for constructing ALHSs. In the FRET process, the presence of a fluorescent acceptor with matching energy levels is crucial. Therefore, for the assembly of ALHSs with PPE-BPI-2CB[7], EsB was selected as the energy acceptor due to its favorable overlap between its absorption band (450–560 nm) and the emission band of PPE-BPI-2CB[7] (420–600 nm) (Fig. S9 in Supporting information). As illustrated in Fig. 2a, the emission peak of PPE-BPI-2CB[7] at 500 nm notably decreased upon the gradual addition of EsB, while a distinct fluorescence emission peak emerged at 560 nm, corresponding to the fluorescence emission of EsB. Additionally, the CIE 1931 chromaticity coordinates clearly demonstrated a transition in fluorescence emission color from blue-green to yellow in the presence of EsB (Fig. S7). Furthermore, we investigated the energy transfer process of LHS by fluorescence lifetimes, in which the fluorescence lifetimes decreased from 2.43 ns to 2.23 ns (Fig. 2d), which indicated the occurrence of an energy transfer process from PPE-BPI-2CB[7] to EsB, with an energy transfer efficiency (Φ_{ET}) of 55.6%, an antenna effect (AE) of 1.8, and fluorescence quantum yield of 23% (Figs. S12 and S13, and Table S1 in Supporting information).

To further emulate the natural photosynthetic system with multi-step sequential energy transfer, we have selected for SR101 dye as the second energy acceptor, given its strong overlap between its absorption band and the emission band of PPE-BPI-2CB[7]+EsB (Fig. S10 in Supporting information). As depicted in Fig. 2b, the fluorescence intensity of PPE-BPI-2CB[7]+EsB at 560 nm decreased upon the addition of SR101, while the emission of SR101 at 620 nm gradually increased. Simultaneously, the CIE 1931 chromaticity coordinates illustrated a shift in fluorescence color from yellow to orange-yellow (Fig. S7). Moreover, the fluorescence lifetimes decreased from 2.23 ns to 1.86 ns (Fig. 2d), and the Φ_{ET}, AE, and fluorescence quantum yield were calculated to be 16.8%, 4.0, and 35% (Figs. S12 and S13, and Table S1). These findings vividly illustrate the successful construction of an efficient ALHS with two-step sequential energy transfer processes.

To further mimic natural photosynthetic systems with multi-step sequential energy transfer, we investigated the feasibility of preparing a three-step sequential energy transfer system by incorporating the third FRET acceptor Cy5. Cy5 demonstrates significant overlap between its absorption band and the emission band of PPE-BPI-2CB[7]+EsB+SR101 (Fig. S11 in Supporting information). As illustrated in Fig. 2c, the fluorescence intensity of PPE-BPI-2CB[7]+EsB+SR101 decreased at 620 nm upon the addition of Cy5, while the emission of Cy5 at 700 nm gradually increased. Concurrently, the CIE 1931 chromaticity coordinates indicated a shift in fluorescence color from orange-yellow to red (Fig. S7). Furthermore, the fluorescence lifetimes decreased from 1.86 ns to 1.68 ns following the addition of Cy5 (Fig. 2d), and the Φ_{ET}, AE, and fluorescence quantum yield were calculated to be 74.1%, 5.2, and 43% (Figs. S12 and S13, and Table S1). These findings unequivocally demonstrate the successful construction of an efficient ALHS with three-step sequential energy transfer processes.

In order to examine the influence of energy transfer processes on reactive oxygen species (ROS) production, we inves-

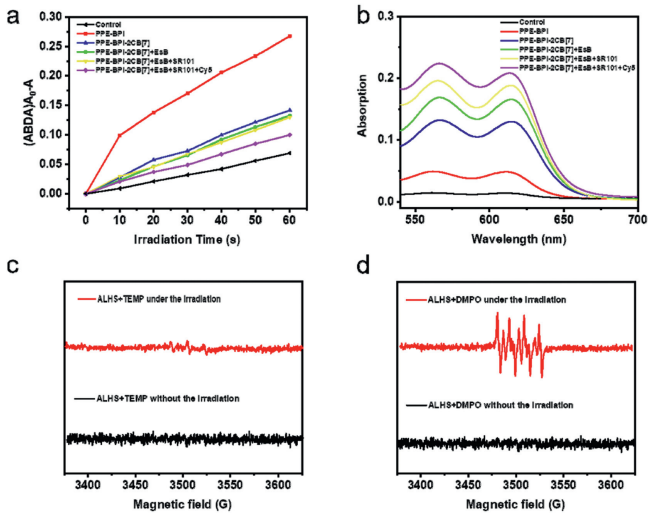

Fig. 3. (a) Plots of ΔAbs (A_0–A) for ABDA at 380 nm upon blue light irradiation for different times in the presence of PPE-BPI, PPE-BPI-2CB[7], PPE-BPI-2CB[7]+EsB, PPE-BPI-2CB[7]+EsB+SR101, and PPE-BPI-2CB[7]+EsB+SR101+Cy5. (b) UV–vis absorption spectra for cationic radicals of TMPD generated by indicated samples under the same conditions. (c) EPR spectra for capturing $^1O_2$ with TEMP serving as the trapping agent in the aqueous solution. (d) EPR spectra for capturing $O_2^{\bullet-}$ with DMPO serving as the trapping agent in the aqueous solution.

tigated the ROS-generating capability of the ALHSs. To explore the types of ROS produced, specific indicators for singlet oxygen ($^1O_2$) and superoxide anion radical ($O_2^{\bullet-}$), namely 9,10-anthracenediylbis(methylene)dimalonic acid (ABDA) and *N,N,N′,N′*-tetramethylphenylenediamine (TMPD), respectively, were employed. Upon irradiating the aqueous solutions of PPE-BPI, PPE-BPI-2CB[7], PPE-BPI-2CB[7]+EsB, PPE-BPI-2CB[7]+EsB+SR101, and PPE-BPI-2CB[7]+EsB+SR101+Cy5 containing ABDA, a decrease in the absorption peak of ABDA was observed of PPE-BPI and other systems remained largely unchanged (Fig. 3a and Fig. S14 in Supporting information), indicating no $^1O_2$ is produced except for PPE-BPI. In contrast, when blue light was used to irradiate the aqueous solutions containing TMPD, all samples caused an increase in the absorption peak of TMPD, with PPE-BPI-2CB[7]+EsB+SR101+Cy5 leading to the strongest increase (Fig. 3b). This observation distinctly indicates that the production of $O_2^{\bullet-}$ is gradually enhanced through a three-step sequential energy transfer process. The generation of $^1O_2$ was further investigated by electron paramagnetic resonance (EPR) measurements with the addition of 2,2,6,6-tetramethylpiperidine (TEMP) as the trapping agent in PPE-BPI-2CB[7]+EsB+SR101+Cy5 solution. Without irradiation, reactive oxygen species (ROS) signal was not detected, while no ROS signal was detected under 425 nm light irradiation (Fig. 3c), which indicating no $^1O_2$ was generated. 5,5-dimethyl-1-pyrroline *N*-oxide (DMPO) was added to PPE-BPI-2CB[7]+EsB+SR101+Cy5 solution as the trapping agent of $O_2^{\bullet-}$ by EPR measurement. No ROS signal was detected without irradiation. Under 425 nm light irradiation, ROS signal was detected (Fig. 3d), indicating that PPE-BPI-2CB[7]+EsB+SR101+Cy5 has excellent $O_2^{\bullet-}$ generation ability.

In order to simulate the entire process of light-harvesting energy transfer, our objective was to employ PPE-BPI-2CB[7]+EsB+SR101+Cy5 as photocatalysts to enhance the photooxidation of *N*-phenyltetrahydroisoquinoline. Table S2 (Supporting information) demonstrates a notable photocatalytic oxidation process of *N*-phenyltetrahydrsisoquinoline, yielding an amazing yield of 86% in water (entry 1). When the photocatalyst is changed to PPE-BPI, PPE-BPI-2CB[7], PPE-BPI-2CB[7]+EsB, and PPE-BPI-2CB[7]+EsB+SR101, the reaction yields decreased to 6%, 18%, 35%, and 42%, respectively (entries 2–5). When CB[7], EsB, SR101 and Cy5 were used as the photocatalysts, the reaction yields decreased to 0%, 14%, 12%, and 8%, respectively (entries 6–9). Reducing the quantity of photocatalyst leads to a diminished reaction yield of 52% (entry 10), whilst increasing it has a minor impact on the reaction yield, resulting in a yield of 88% (entry 11). Reducing the reaction period to 12 h results in a decrease in the reaction yield, with just 47% achieved (entry 12). In contrast, increasing the reaction time to 24 h has a little impact on the reaction yield, resulting in a yield of 87% (entry 13). The lack of both photocatalyst and light hinders the desired reaction from taking place, indicating that both components are essential requirements for the reaction to proceed effectively (entries 14 and 15).

In order to evaluate the appropriateness of PPE-BPI-2CB[7]+EsB+SR101+Cy5 as a photocatalyst for improving the photooxidation of *N*-phenyltetrahydroisoquinoline in water, various substrates were used in the reaction. Scheme 2 illustrates that PPE-BPI-2CB[7]+EsB+SR101+Cy5 significantly enhances the properties of several *N*-phenyltetrahydroisoquinoline derivatives with diverse substituents (-CH_3, -NO_2, -F, -Cl, -Br, –OCH_3) to give yields of 83% (**2b**), 69% (**2c**), 81% (**2d**), 82% (**2e**), 80% (**2f**), and 87% (2g). The substitution of phenyl with naphthalene led to reaction yields of 71% (2h), 72% (**2i**), and 74% (**2j**). Moreover, to study the mechanism of the photooxidation reaction, we also studied the active species in the catalytic reaction catalyzed by the PPE-BPI-2CB[7]+EsB+SR101+Cy5 system. The mechanism of the photooxidation reaction showed that the introduction of 1,4-benzoquinone (BQ) resulted in a significant decrease in the yield of the *N*-phenyltetrahydroisoquinoline photooxidation reaction, which was only 13% of the yield. However, under the same reaction conditions, the addition of sodium azide (NaN_3), triethylamine (TEA), and potassium iodide (KI) had no significant effect on the reaction yield, indicating that $O_2^{\bullet-}$ is the main active species in the photooxidizing *N*-phenyltetrahydroisoquinoline (Fig. S15 in Supporting information). In addition, the Stern-Volmer quenching studies confirmed a decrease emission intensity quenching of PPE-BPI-2CB[7]+EsB+SR101+Cy5 by *N*-phenyltetrahydroisoquinoline (quenching constant, $k_q = 3.15 \times 10^8$ L mol^{-1} s^{-1}) (Fig. S16 in Supporting information). Based on our prior research [56], we put forward a credible photocatalytic process (Scheme 3). When exposed to light, the excited state [PPE-BPI-2CB[7]]* transfers energy to the acceptor dye, leading to the creation of the excited state [EsB]*. Afterwards, energy is transferred from [EsB]* to [SR101], resulting in the production of [SR101]*, and subsequently [Cy5]*. This leads to direct electron transfer with triplet oxygen ($^3O_2$), finally producing $O_2^{\bullet-}$ and $[Cy5]^{\bullet+}$. The substrate undergoes a reaction with $O_2^{\bullet-}$ to produce an intermediate nitrogen radical anion I. At the same time, another *N*-phenyltetrahydroisoquinoline compound decreases the concentration of $[Cy5]^{\bullet+}$ and produces both intermediate I and the normal state of [Cy5]. Moreover, intermediate I undergoes a hydrogen atom transfer (HAT) process with $O_2^{\bullet-}$ to generate alkyl radical intermediate II. Ultimately, II undergoes a reaction with $O_2^{\bullet-}$ and, upon elimination of H_2O, produces the ultimate product.

In conclusion, we present a novel three-step sequential energy transfer mechanism, orchestrated *via* host-guest interactions between a piperazine derivative (PPE-BPI) exhibiting AIE properties and CB[7] in an aqueous medium, serving as adept energy donors. To enact this sequential energy transfer, we enlist three distinct fluorescent dyes, EsB, SR101, and Cy5, as energy acceptors. The PPE-PBI-2CB[7]+EsB+SR101+Cy5 system elegantly demonstrates a remarkably efficient three-step energy transfer cascade, commencing with PPE-PBI-2CB[7] and sequentially channeling energy to EsB, SR101, and culminating with Cy5, showcasing exceptional energy transfer efficiencies. Intriguingly, as energy traverses this multi-step pathway, the generation efficiency of $O_2^{\bullet-}$ steadily escalates. These radicals hold promise as photocatalysts for the selective pho-

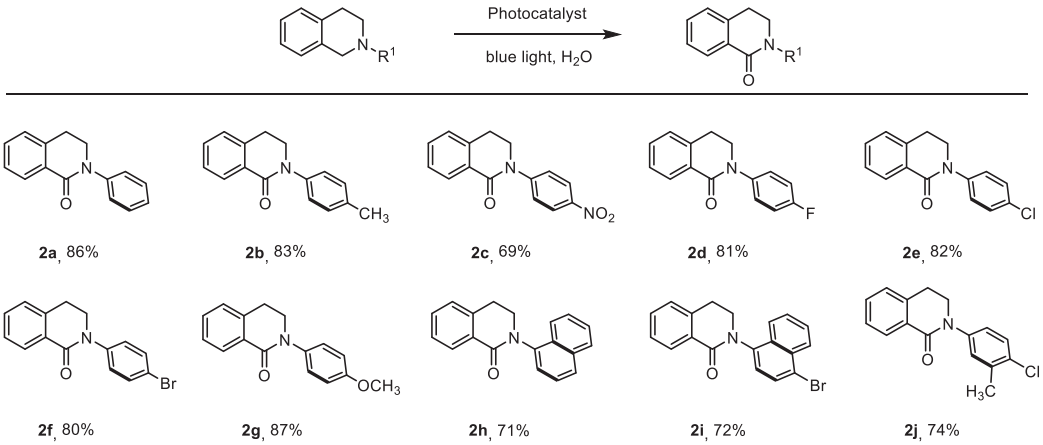

Scheme 2. Substrate scope with respect to *N*-phenyltetrahydroisoquinoline derivatives. Standard conditions: *N*-phenyltetrahydroisoquinoline (0.2 mmol), PPE-BPI-2CB[7]+EsB+SR101+Cy5 (0.5 mol%), H_2O (2.0 mL), 425 nm blue light, room temperature, 18 h, isolated yield.

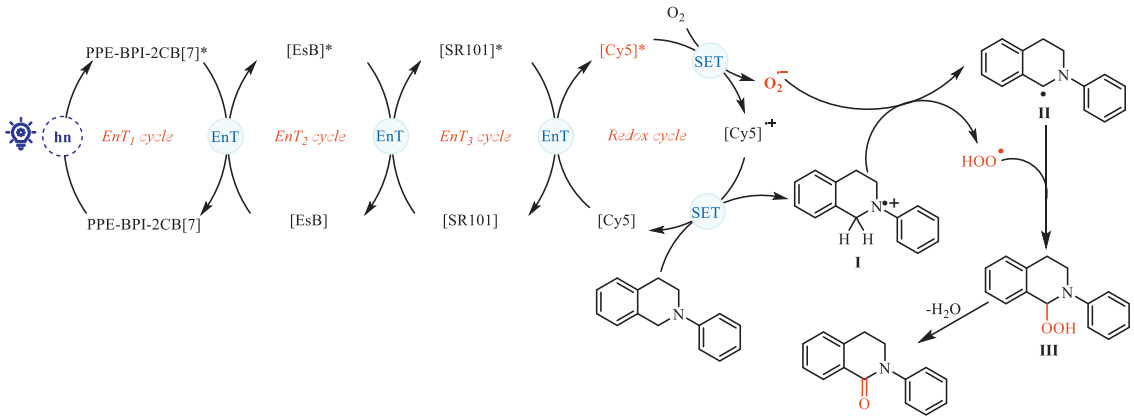

Scheme 3. Proposed mechanism for photooxidation of *N*-phenyltetrahydroisoquinoline.

tooxidation of *N*-phenyltetrahydroisoquinoline in an aqueous solution, yielding an impressive 86% yield after 18 h of irradiation. This investigation represents a significant stride towards emulating and understanding multi-step energy transfer phenomena inherent in nature, charting a course for further exploration in this domain.

Declaration of competing interest

The authors declare that they have no known competing financial interests or personal relationships that could have appeared to influence the work reported in this paper.

CRediT authorship contribution statement

Yusong Bi: Methodology, Investigation, Formal analysis. **Rongzhen Zhang:** Investigation, Formal analysis, Data curation. **Kaikai Niu:** Investigation, Data curation. **Shengsheng Yu:** Formal analysis, Data curation. **Hui Liu:** Methodology, Formal analysis, Data curation. **Lingbao Xing:** Writing – review & editing, Supervision, Resources, Funding acquisition, Conceptualization.

Acknowledgments

We are grateful for the financial support from the National Natural Science Foundation of China (No. 52205210) and the Natural Science Foundation of Shandong Province (Nos. ZR2020MB018, ZR2022QE033 and ZR2021QB049).

Supplementary materials

Supplementary material associated with this article can be found, in the online version, at doi:10.1016/j.cclet.2024.110311.

References

[1] H.Q. Peng, L.Y. Niu, Y.Z. Chen, et al., Chem. Rev. 115 (2015) 7502–7542.
[2] G. McDermott, S. Prince, A. Freer, et al., Nature 374 (1995) 517–521.
[3] G.D. Scholes, G.R. Fleming, A. Olaya-Castro, et al., Nat. Chem. 3 (2011) 763–774.
[4] A.M. van Oijen, M. Ketelaars, J. Köhler, et al., Science 285 (1999) 400–402.
[5] O. Dumele, J. Chen, J.V. Passarelli, et al., Adv. Mater. 32 (2020) 1907247.
[6] Y.X. Hu, W.J. Li, P.P. Jia, et al., Adv. Opt. Mater. 8 (2020) 2000265.
[7] S. Kundu, A. Patra, Chem. Rev. 117 (2017) 712–757.
[8] K. Wang, K. Velmurugan, B. Li, et al., Chem. Commun. 57 (2021) 13641–13654.
[9] T. Xiao, W. Zhong, L. Zhou, et al., Chin. Chem. Lett. 30 (2019) 31–36.
[10] K. Wang, Y. Shen, P. Jeyakkumar, et al., Curr. Opin. Green Sustain. 41 (2023) 100823.
[11] X.M. Chen, X. Chen, X.F. Hou, et al., Nanoscale Adv. 5 (2023) 1830–1852.
[12] C.H. Wu, P.Q. Nhien, T.T.K. Cuc, et al., Top Curr. Chem. 381 (2022) 2.
[13] D. Bokotial, K. Acharyya, A. Chowdhury, et al., Angew. Chem. Int. Ed. 63 (2024) e202401136.
[14] Q. Zhang, H. Qian, T. Xiao, et al., Chin. Chem. Lett. 34 (2023) 108365.
[15] T. Xiao, X. Li, L. Zhang, et al., Chin. Chem. Lett. 35 (2024) 108618.
[16] Z. Wu, H. Qian, X. Li, et al., Chin. Chem. Lett. 35 (2024) 108829.
[17] H.Q. Peng, Y.Z. Chen, Y. Zhao, et al., Angew. Chem. Int. Ed. 51 (2012) 2088–2092.
[18] M. Kownacki, S.M. Langenegger, S.X. Liu, et al., Angew. Chem. Int. Ed. 58 (2019) 751–755.
[19] J.J. Li, Y. Chen, J. Yu, et al., Adv. Mater. 29 (2017) 1701905.
[20] Z. Zhang, Z. Zhao, Y. Hou, et al., Angew. Chem. Int. Ed. 58 (2019) 8862–8866.
[21] K. Acharyya, S. Bhattacharyya, H. Sepehrpour, et al., J. Am. Chem. Soc. 141 (2019) 14565–14569.
[22] Y. Li, Y. Dong, L. Cheng, et al., J. Am. Chem. Soc. 141 (2019) 8412–8415.
[23] C. Vijayakumar, K. Sugiyasu, M. Takeuchi, Chem. Sci. 2 (2011) 291–294.

[24] Y. Liu, J. Jin, H. Deng, et al., Angew. Chem. Int. Ed. 55 (2016) 7952–7957.
[25] C.B. Huang, L. Xu, J.L. Zhu, et al., J. Am. Chem. Soc. 139 (2017) 9459–9462.
[26] S. Garain, B.C. Garain, M. Eswaramoorthy, et al., Angew. Chem. Int. Ed. 60 (2021) 19720–19724.
[27] L. Xu, Z. Wang, R. Wang, et al., Angew. Chem. Int. Ed. 59 (2020) 9908–9913.
[28] J. Pruchyathamkorn, W.J. Kendrick, A.T. Frawley, et al., Angew. Chem. Int. Ed. 59 (2020) 16455–16458.
[29] X.M. Chen, Q. Cao, H.K. Bisoyi, et al., Angew. Chem. Int. Ed. 59 (2020) 10493–10497.
[30] H.J. Kim, D.R. Whang, J. Gierschner, et al., Angew. Chem. Int. Ed. 55 (2016) 15915–15919.
[31] S. Guo, Y. Song, Y. He, et al., Angew. Chem. Int. Ed. 57 (2018) 3163–3167.
[32] Z. Xu, S. Peng, Y.Y. Wang, et al., Adv. Mater. 28 (2016) 7666–7671.
[33] S. Yu, R.X. Zhu, K.K. Niu, et al., Chem. Sci. 15 (2024) 1870–1878.
[34] L.B. Xing, Y. Wang, X.L. Li, et al., Adv. Opt. Mater. 11 (2023) 2201710.
[35] Y. Wang, C.Q. Ma, X.L. Li, et al., J. Mater. Chem. A 11 (2023) 2627–2633.
[36] Y. Wang, N. Han, X.L. Li, et al., ACS Appl. Mater. Interfaces 14 (2022) 45734–45741.
[37] Z. Zhang, Z. Zhao, L. Wu, et al., J. Am. Chem. Soc. 142 (2020) 2592–2600.
[38] X.H. Wang, N. Song, W. Hou, et al., Adv. Mater. 31 (2019) 1903962.
[39] D. Zhang, Y. Liu, Y. Fan, et al., Adv. Funct. Mater. 26 (2016) 7652–7661.
[40] C. Ma, Y. Wang, N. Han, et al., Chin. Chem. Lett. 35 (2024) 108632.
[41] Y. Sun, F. Guo, T. Zuo, et al., Nat. Commun. 7 (2016) 12042.
[42] H. Qian, T. Xiao, R. Elmes, et al., Chin. Chem. Lett. 34 (2023) 108185.
[43] C. Ma, N. Han, Y. Wang, et al., Chin. Chem. Lett. 34 (2023) 108081.
[44] Y. Wang, N. Han, X. Li, et al., ChemPhysMater 1 (2022) 281–293.
[45] Z. Wu, H. Qian, X. Li, et al., Chin. Chem. Lett. 35 (2023) 108829.
[46] D. Chen, T. Xiao, E. Monflier, et al., Commun. Chem. 7 (2024) 88.
[47] L. Ji, Y. Sang, G. Ouyang, et al., Angew. Chem. Int. Ed. 58 (2019) 844–848.
[48] Q. Song, S. Goia, J. Yang, et al., J. Am. Chem. Soc. 143 (2020) 382–389.
[49] M. Hao, G. Sun, M. Zuo, et al., Angew. Chem. Int. Ed. 59 (2020) 10095–10100.
[50] P.P. Jia, L. Xu, Y.X. Hu, et al., J. Am. Chem. Soc. 143 (2021) 399–408.
[51] D. Zhang, W. Yu, S. Li, et al., J. Am. Chem. Soc. 143 (2021) 1313–1317.
[52] Y. Li, C. Xia, R. Tian, et al., ACS Nano 16 (2022) 8012–8021.
[53] M. Suresh, A.K. Mandal, E. Suresh, et al., Chem. Sci. 4 (2013) 2380–2386.
[54] D. Ren, L. Tang, Z. Wu, et al., Chin. Chem. Lett. 34 (2023) 108617.
[55] D. Zhang, M. Li, B. Jiang, et al., J. Colloid Interface Sci. 652 (2023) 1494–1502.
[56] X.Y. Yao, S. Yu, R.Z. Zhang, et al., Sci. China Mater. 67 (2024) 833–841.